

Fig. 6. Typical failure patterns of RAC-FSSTs.

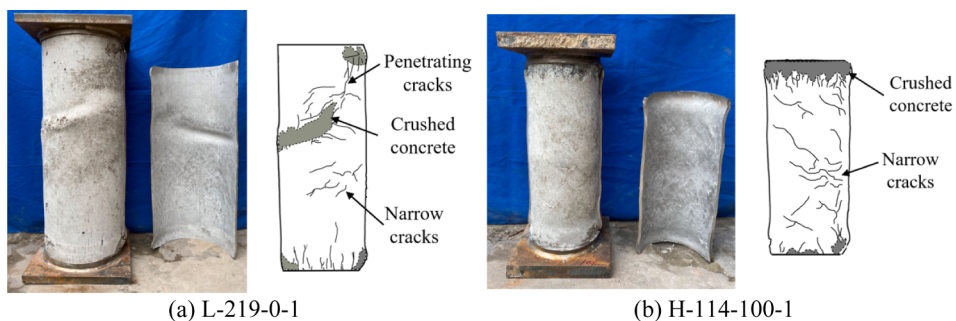


Fig. 7. Core concrete damage.

strength and Young's modulus losses. For example, for concrete with w/c ratio of 0.49, the compressive strengths containing 50% and 100% CRA respectively declined 7.0% and 4.9% as compared with NAC, while 17.6% and 22.8% reductions in Young's modulus are observed. An obvious loss of elastic modulus with the incorporation of CRAs is found. This was primarily caused by the lower elastic modulus of residual mortar adhered to the original aggregate [36,37].

All employed tubes were cut from the seamless steel tube, see Fig. 4(a). To ensure that the infilled concrete and stainless steel tube worked together under axial load, the RAC-FSST specimens were prepared as follows: Firstly, a 20 mm thick steel plate was welded to the bottom end of the tube before concrete pouring. Then the concrete was casted slightly higher than the tube and after 28 d curing, the top of the concrete was ground to achieve a smooth and flat surface (Fig. 4(b)). Finally, the other steel plate was welded. All specimens before testing are presented in Fig. 4(c).

2.3. Experimental setup and measurement

Experiments were performed using a 5000 kN hydraulic compression machine. Fig. 5 presents the test scene and schematic view of the whole loading set-up and instrumentation arrangements. The axial deformations of the specimens were measured using 4 LVDTs. Eight strain gauges were used to measure the vertical and circumferential strains at the mid height of the columns.

Before compression, the specimen was adjusted to ensure that the load was concentrically applied. A preloading stage was conducted within the range of 30% of the estimated load-bearing capacity. During the initial loading phase, the specimens were loaded with a speed of 1 kN/s and the load interval was set as 100 kN. When the load reached 70% of the estimated strength, the displacement-control loading with a rate of 1 mm/min was employed until failure. Due to the greater

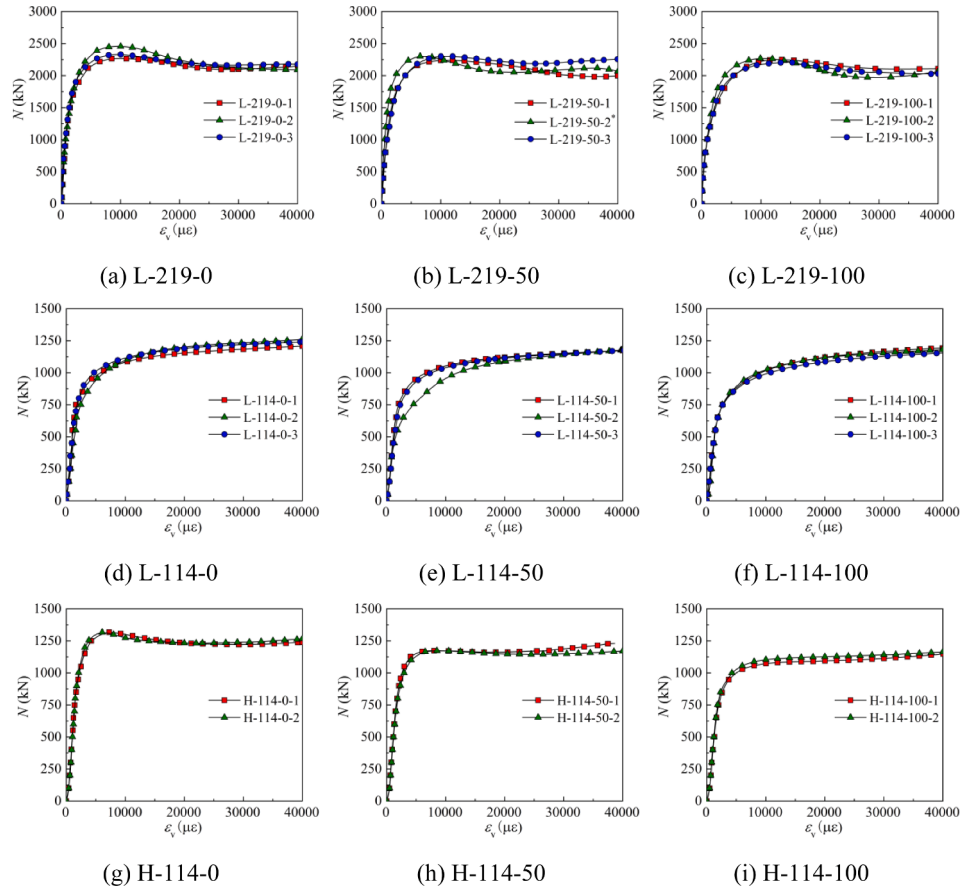
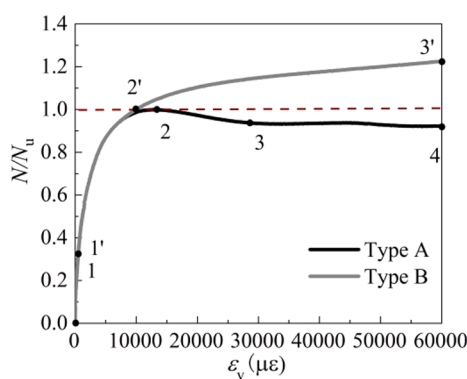
ductility of CFSTs with external stainless steel tube [38,39], the load may increase continuously even though the axial strain was very large. For comparison purpose, the test was terminated when the axial shortening reached 20 mm and 40 mm for specimens with diameters of 114 mm and 219 mm, respectively.

3. Experimental results and analysis

3.1. Failure pattern

Fig. 6 presents the typical failure patterns of RAC-FSSTs, which can be categorized into 2 types. The specimens with steel ratio of 7.5% showed typical shear failure and the outward buckling occurred at the position of one end and the mid-height. The angles between failure and horizontal planes were around 55°–60°. For specimens with higher steel ratio of 16.5%, the drum-like deformation exhibited at the mid-height and ends of specimens. Similar failure patterns were found in specimens with varying CRA contents and concrete strengths.

After testing, the stainless tube was cut into halve and removed. The damage of infilled RAC was then observed. Fig. 7 gives the photos and schematic diagram of concrete damage for the representative Samples L-219-0-1 and H-114-100-1. As shown, the crushed concrete was observed at the position that the occurrence of outward buckling. Several narrow cracks were located at around 1/3 height of the specimens. More microcracks were observed for Sample H-114-100-1 with higher steel ratio, which illustrated that stronger confinement effect could effectively restrained occurrence of penetrating cracks. In general, the inner concrete remained good integrity. Similar failure patterns were found among specimens with different CRA content. In addition, no scratch was observed at the internal surface of the tube, indicating that the stainless steel tube and core concrete worked together under the axial load.

Fig. 8. Axial load (N) vs. vertical strain (ε_v) curves of RAC-FSSTs.Fig. 9. Typical N - ε_v curves of RAC-FSSTs under axial load.

3.2. Axial load vs. Strain responses

The axial load vs. strain responses of all specimens are illustrated in Fig. 8. As presented, the usage of RAC had an insignificant effect on the development trends of the stress-strain curves. In general, the responses of N - ε_v can be divided into 2 types, as shown in Fig. 9, which is mainly related to the confinement effect. For the specimens with steel ratio α of 7.5%, the type A curves were presented, mainly including the elastic (0-1), elastic-plastic (1-2), declining (2-3) and nearly horizontal (3-4) portions. As the value of α increases to 16.5%, the N - ε_v curves exhibit an obvious strain-hardening behaviour (2'-3') after an elastic-plastic phase (type B). These two types of curves indicate that the stainless steel tube could provide a good confinement on the core concrete at large axial strain.

3.3. Influence of CRA replacement

As distinguished from the similar development trends of N - ε_v curves,

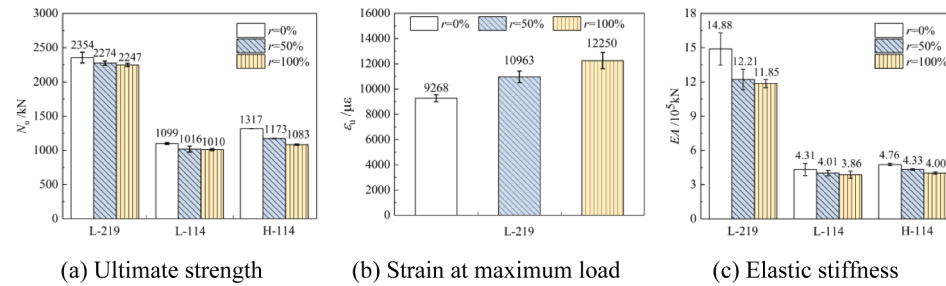
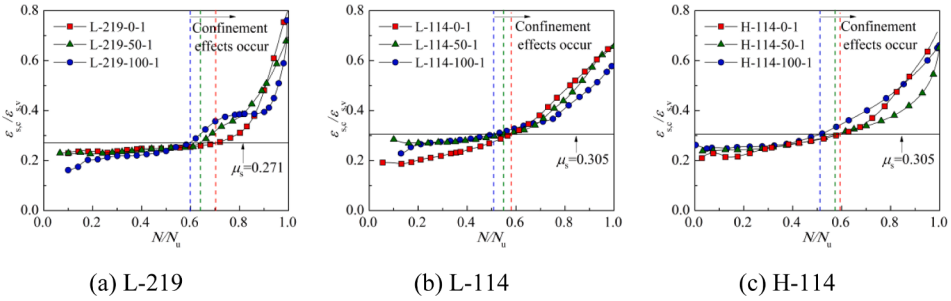
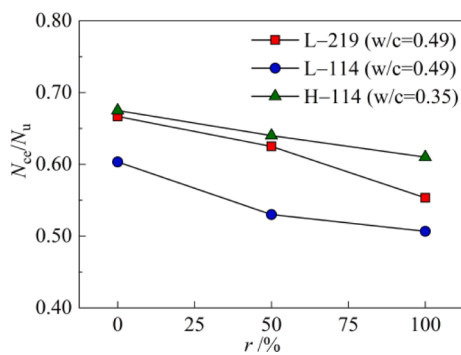


Fig. 10. Influence of CRA replacement levels.

Fig. 11. Evolutions of $\epsilon_{s,c}/\epsilon_{s,v}$ for different types of specimens.Fig. 12. Effects of CRA content on N_{ce}/N_u .

the elastic stiffness (EA), ultimate strength (N_u) and corresponding strain (ϵ_u) are affected by CRA content in different degree. For curves without a declining portion, the N_u is taken as the load corresponding to 1% axial strain for comparison, as suggested by Uy et al. [17] and Wang et al.

[40]. The secant modulus at 40% of N_u is defined as the EA.

Fig. 10(a)-(c) illustrate the variations of the N_u , ϵ_u and EA along with the CRA replacement level, respectively. The error bars denoting the standard deviation are also given in the figures to reflect the data scatter. As presented in Fig. 10(a), the values of N_u were moderately affected by the CRA replacements for RAC-FSST samples with 0.49 w/c ratio concrete. The difference of 3.4% and 4.5% were observed for the N_u when the replacement level rose from 0% to 50% and 100% for Samples L-219. Similar moderate influence of CRA content on the N_u also has also been found in other types of CFST members [12,41,42]. However, the maximum difference of 17.8% was observed for the N_u when the replacement level rose from 0% to 100% for samples with 0.35 w/c ratio concrete (H-114). For the EA and ϵ_u , the incorporation of CRA obviously affected these two indexes. As the CRA replacement rose, the value of EA declined, while the ϵ_u increased. For example, when the CRA replacement rose from 0% to 100%, the values of EA and ϵ_u for Samples L-219 decreased by 20.4% and increased by 32.2%, respectively. Test results indicated that the incorporation of CRA resulted in the lower axial stiffness and larger strain at N_u , which was mainly due to the lower stiffness of the CRA induced by attached old mortar. Generally, the

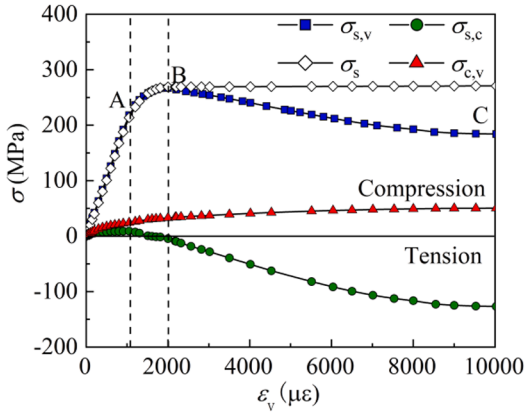
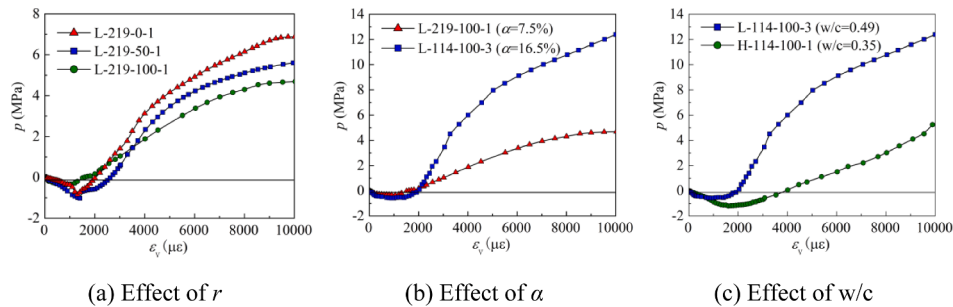
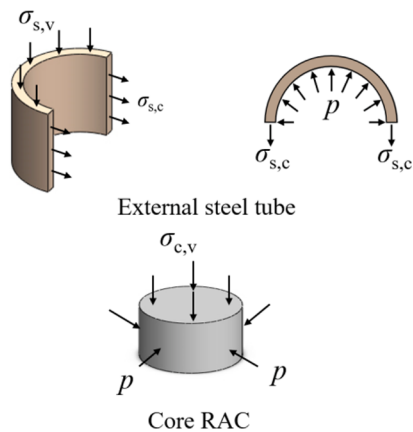
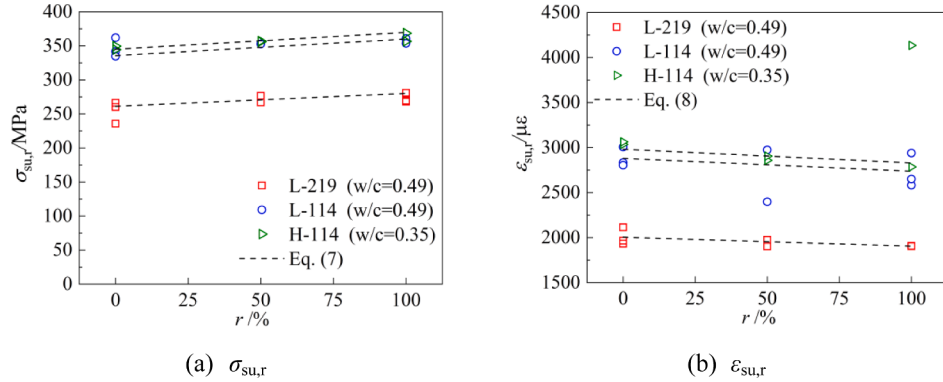
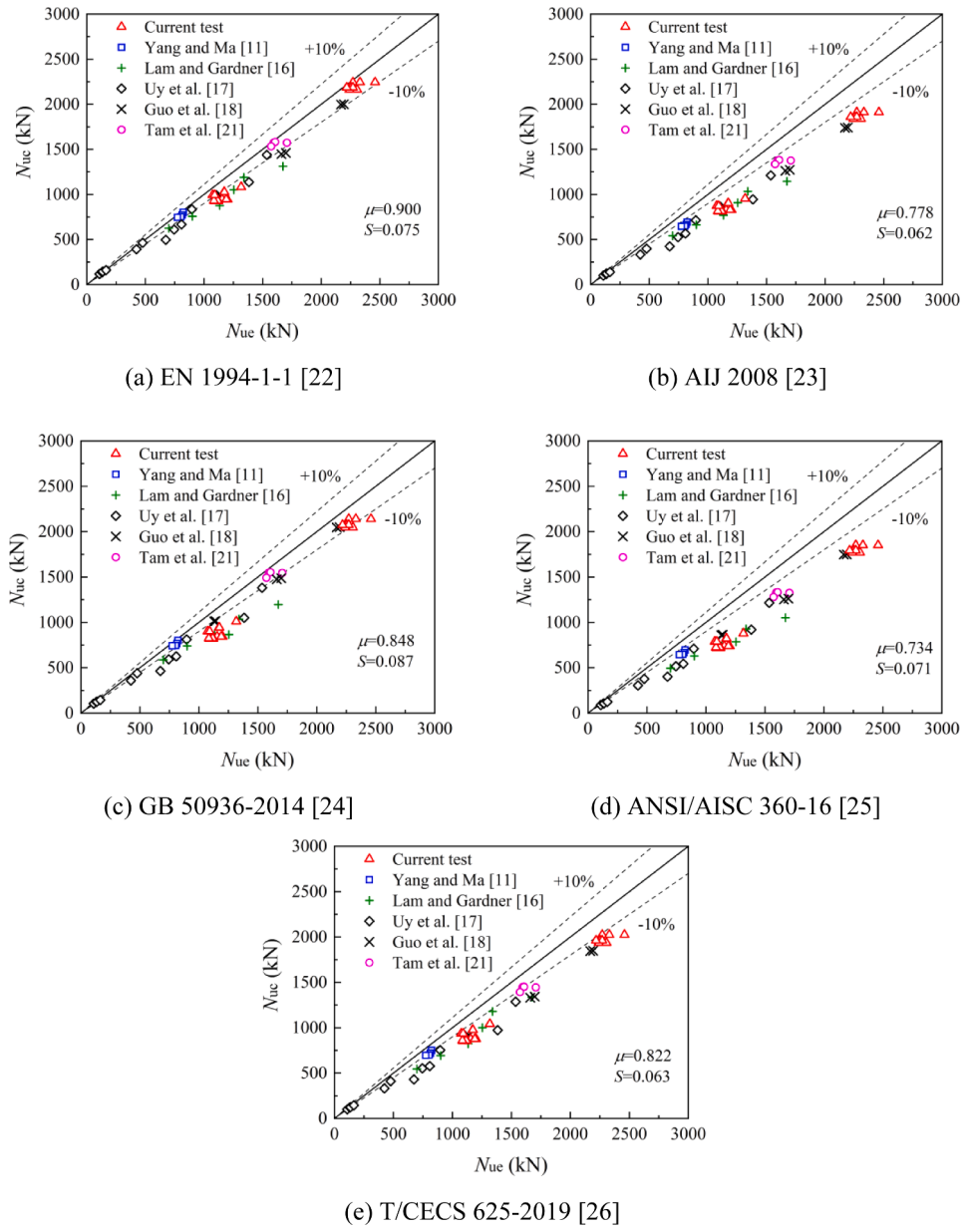


Fig. 13. Stress states of stainless steel tube and core RAC for Sample L-219-100-1.

Fig. 14. Developments of p for samples with different parameters.

Fig. 15. Influences of CRA content on $\sigma_{su,r}$ and $\epsilon_{su,r}$.Fig. 16. Evaluations of N_u to RAC-FSSTs by available design codes.

in which μ_{sp} is the Poisson's ratio during elastic-plastic phase, E_s^t is the tangent modulus of stainless steel, which declined from E_0 to $E_{0.2}$ and σ_s is equivalent stress.

A.2.3. Starin hardening stage: $\sigma_s > \sigma_{0.2}$

$$\begin{bmatrix} d\sigma_{s,c} \\ d\sigma_{s,v} \end{bmatrix} = \frac{E_0}{Q} \begin{bmatrix} \dot{\sigma}_v + 2p & -\dot{\sigma}_v \dot{\sigma}_c + 2\mu_{sp} \\ -\dot{\sigma}_v \dot{\sigma}_c + 2\mu_{sp} & \dot{\sigma}_v + 2p \end{bmatrix} \begin{bmatrix} d\varepsilon_{s,c} \\ d\varepsilon_{s,v} \end{bmatrix} \quad 2.7)$$

$$\dot{\sigma}_v = \sigma_{s,v} - \sigma_m \quad 2.8)$$

$$\dot{\sigma}_c = \sigma_{s,c} - \sigma_m \quad 2.9)$$

$$\sigma_m = (\sigma_{s,v} + \sigma_{s,c})/3 \quad 2.10)$$

$$p = \frac{2H}{9E_0} \dot{\sigma}^2 \quad 2.11)$$

$$H = \frac{d\sigma}{d\varepsilon_p} = 10^{-3} E_0^2 \quad 2.12)$$

$$Q = \dot{\sigma}_c^2 + \dot{\sigma}_v^2 + 2\mu_s \dot{\sigma}_c \dot{\sigma}_v + 2H(1-\mu_s) \dot{\sigma}_s^2 / 9G \quad 2.13)$$

$$G = \frac{E_0}{2(1+\mu_s)} \quad 2.14)$$

where $\dot{\sigma}_v$ and $\dot{\sigma}_c$ are deviatoric stresses in vertical and circumferential directions, respectively, σ_m is the mean stress, G refers to the shear modulus.

Appendix B. Comparisons between test curves and proposed vertical stress-strain relationships of RAC-FSSTs

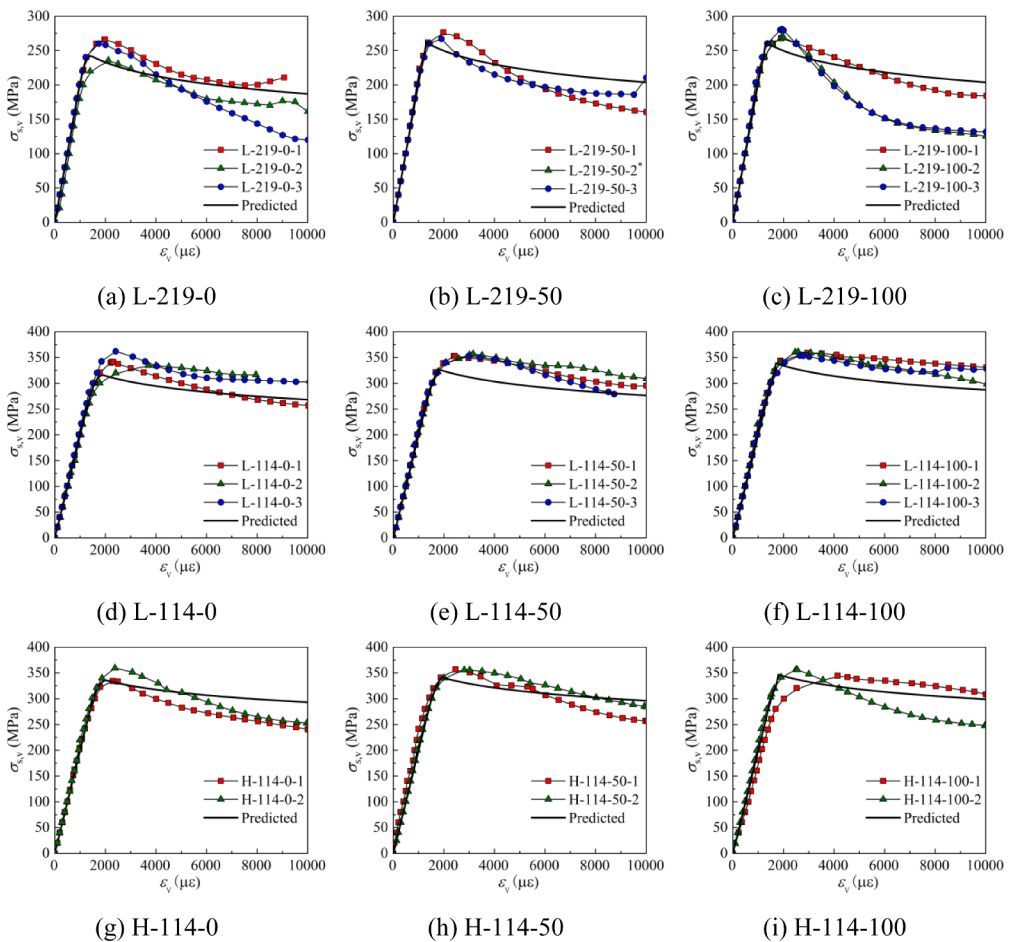


Fig. B1. Comparisons between test curves and $\sigma_{s,v}$ - ε_v relationships of external steel tube.

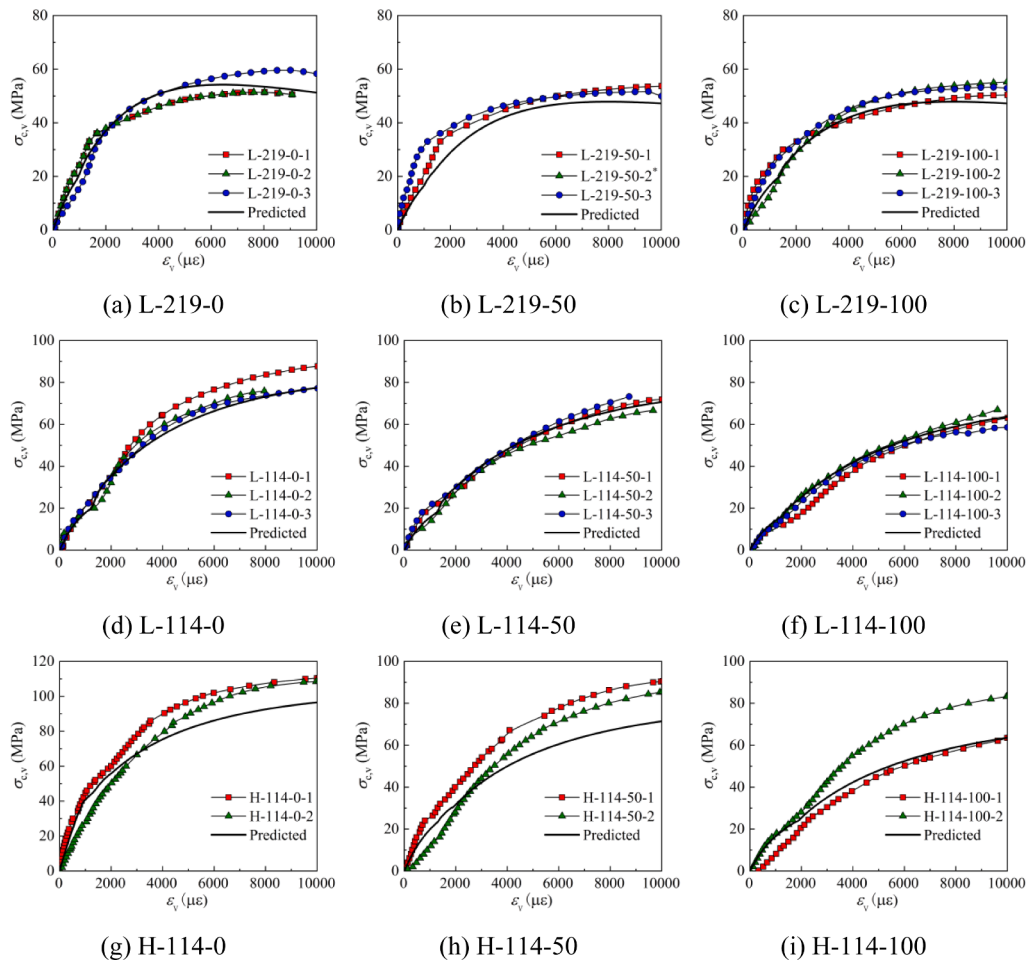


Fig. B2. Comparisons between test curves and $\sigma_{cv}-\varepsilon_v$ relationships of core RAC.

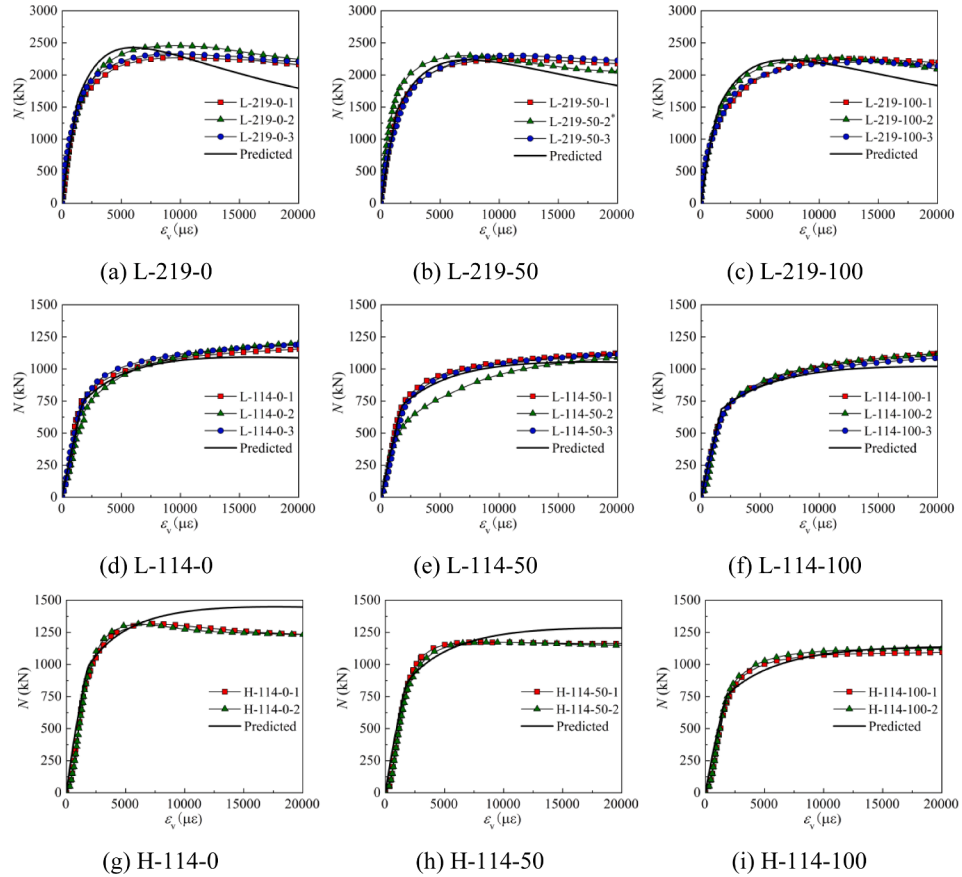


Fig. B3. Comparisons between test curves and $N-\varepsilon_v$ models of RAC-FSSTs and CFSSTs: (a)-(i) from this study; (j)-(m) from Yang and Ma [11]; (n)-(q) from Tam et al. [21]; (r)-(t) from Guo et al. [18].

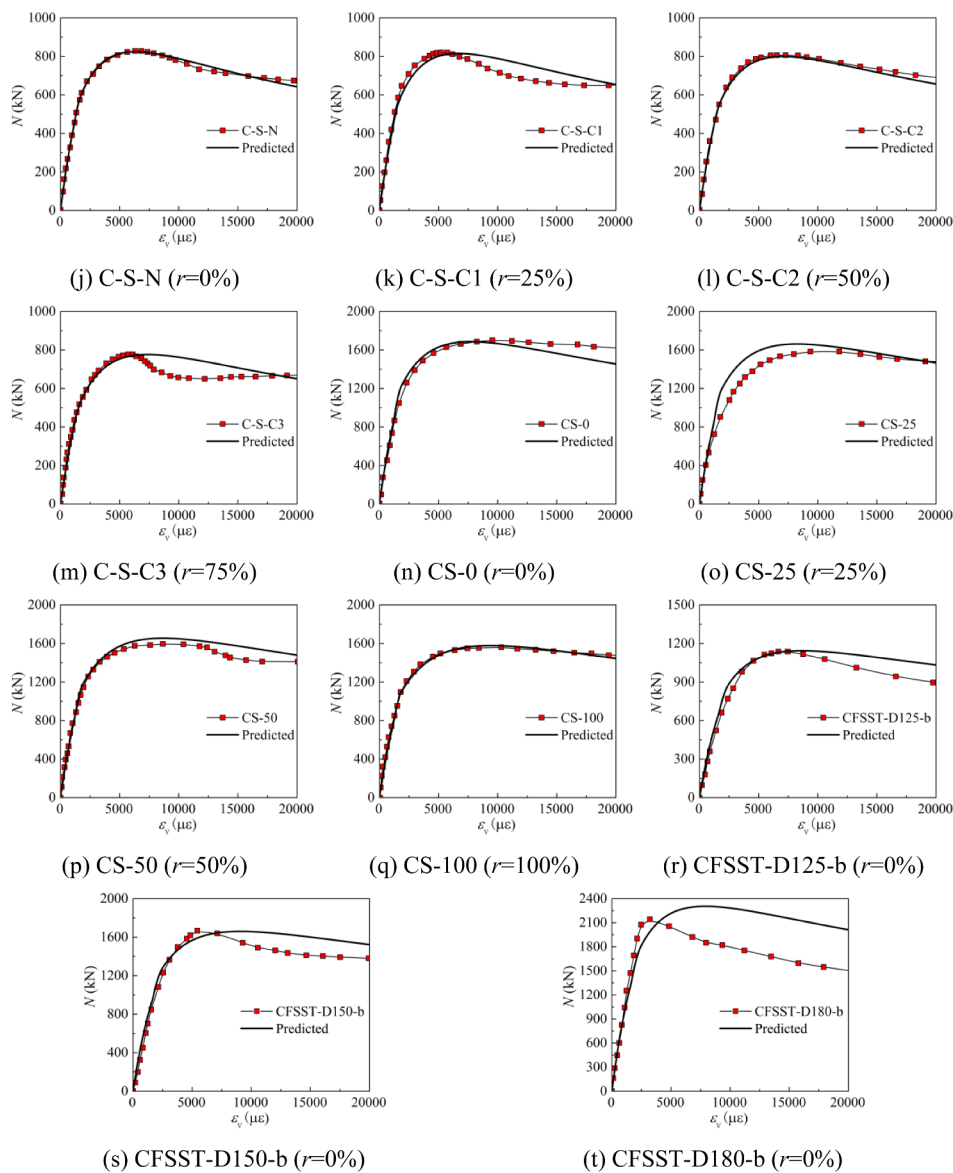


Fig. B33. (continued).

References

- [1] Young B, Ellobody E. Experimental investigation of concrete-filled cold-formed high strength stainless steel tube columns. *J Constr Steel Res* 2006;62(5):484–92.
- [2] Han L-H, Chen F, Liao F-Y, Tao Z, Uy B. Fire performance of concrete filled stainless steel tubular columns. *Eng Struct* 2013;56:165–81.
- [3] Han LH, Xu CY, Tao Z. Performance of concrete filled stainless steel tubular (CFSST) columns and joints: Summary of recent research. *J Constr Steel Res* 2019; 152:117–31.
- [4] Zhao H, Wang R, Hou CC, Lam D. Performance of circular CFDST members with external stainless steel tube under transverse impact loading. *Thin-Walled Struct* 2019;145:106380.
- [5] Zhao H, Wang R, Lam D, Hou C-C, Zhang R. Behaviours of circular CFDST with stainless steel external tube: Slender columns and beams. *Thin-Walled Struct* 2021; 158:107172. <https://doi.org/10.1016/j.tws.2020.107172>.
- [6] Chen Z, Xu J, Xue J, Su Y. Performance and calculations of recycled aggregate concrete-filled steel tubular (RACFST) short columns under axial compression. *Int J Steel Struct* 2014;14(1):31–42.
- [7] Geng Y, Wang Y, Chen J. Time-dependent behaviour of steel tubular columns filled with recycled coarse aggregate concrete. *J Constr Steel Res* 2016;122:455–68.
- [8] Wang Y-Y, Geng Y, Chang Y-C, Zhou C-J. Time-dependent behaviour of recycled concrete filled steel tubes using RCA from different parent waste material. *Constr Build Mater* 2018;193:230–43.
- [9] Lyu W-Q, Han L-H. Investigation on bond strength between recycled aggregate concrete (RAC) and steel tube in RAC-filled steel tubes. *J Constr Steel Res* 2019; 155:438–59.
- [10] He A, Su A, Liang Y, Zhao O. Experimental and numerical investigations of circular recycled aggregate concrete-filled stainless steel tube columns. *J Constr Steel Res* 2021;179:106566.
- [11] Yang Y-F, Ma G-L. Experimental behaviour of recycled aggregate concrete filled stainless steel tube stub columns and beams. *Thin-Walled Struct* 2013;66:62–75.
- [12] Wang Y, Chen J, Geng Y. Testing and analysis of axially loaded normal-strength recycled aggregate concrete filled steel tubular stub columns. *Eng Struct* 2015;86: 192–212.
- [13] Zhao MZ, Wang YY, Lehman DE, Geng Y, Roeder CW. Response and modeling of axially-loaded concrete-filled steel columns with recycled coarse and fine aggregate. *Eng Struct* 2021;234:111733.
- [14] Lyu WQ, Han LH, Hou C. Axial compressive behaviour and design calculations on recycled aggregate concrete-filled steel tubular (RAC-FST) stub columns. *Eng Struct* 2021;241:112452.
- [15] Azevedo Vda Sde, Lima LROde, Vellasco PCGda S, Tavares MEdaN, Chan TM. Experimental investigation on recycled aggregate concrete filled steel tubular stub columns under axial compression. *J Constr Steel Res* 2021;187:106930.
- [16] Lam D, Gardner L. Structural design of stainless steel concrete filled columns. *J Constr Steel Res* 2008;64(11):1275–82.
- [17] Uy B, Tao Z, Han L-H. Behaviour of short and slender concrete-filled stainless steel tubular columns. *J Constr Steel Res* 2011;67(3):360–78.
- [18] Guo L, Liu Y, Fu F, Huang H. Behavior of axially loaded circular stainless steel tube concrete-filled stub columns. *Thin-Walled Struct* 2019;139:66–76.
- [19] Patel VI, Liang QQ, Hadji MNS. Nonlinear analysis of axially loaded circular concrete-filled stainless steel tubular short columns. *J Constr Steel Res* 2014;101: 9–18.

